Wind Forced Wave–Mean Flow Interactions in the Equatorial Waveguide. Part I: The Kelvin Wave

LEWIS M. ROTHSTEIN

School of Oceanography, University of Washington, Seattle, Washington

MICHAEL J. MCPHADEN

NOAA/Pacific Marine Environmental Laboratory, Seattle, Washington

JEFFREY A. PROEHL

School of Oceanography, University of Washington, Seattle, Washington

(Manuscript received 7 April 1987, in final form 11 April 1988)

ABSTRACT

A numerical model is designed to study the effects of the strong, near-surface shears associated with the equatorial current system on energy transmission of time-periodic equatorial waves into the deep ocean. The present paper is confined to long wavelength, low-frequency Kelvin waves forced by a longitudinally confined patch of zonal wind. Energy transmission into the deep ocean is investigated as a function of mean current shear amplitude and geometry and the forcing frequency.

Solutions form well-defined beams of energy that radiate energy eastward and vertically toward the deep ocean in the absence of mean flow. However, the presence of critical surfaces associated with mean currents inhibits low-frequency energy from reaching the deep ocean. For a given zonal wavenumber, longitudinal propagation through mean currents will be less inhibited as the frequency increases (phase speed increases). When the mean current amplitude is large enough, the beam encounters multiple critical surfaces (i.e., critical surfaces for different wavenumber components of the beam) where significant exchanges of energy and momentum can take place with the mean currents via Reynolds stress transfers. Work against the mean vertical shear is the dominant wave energy loss for the case of a mean South Equatorial Current–Equatorial Undercurrent system, illustrating the need for high vertical resolution in equatorial ocean models.

The model also describes the possible induction of a mean zonal acceleration as well as a mean meridional circulation. Eliassen-Palm fluxes are used to diagnose these dynamics. The presence of critical surfaces result in mean field accelerations on the equator above the core of the Equatorial Undercurrent. Implications of these results with regard to observations in the equatorial waveguide are discussed.

1. Introduction

The discovery of deep equatorial zonal flows in the Indian Ocean (Luyten and Swallow 1976) and later in the Pacific Ocean (Hayes and Milburn 1980; Eriksen 1981) stimulated a great deal of interest in the dynamics of the deep equatorial oceans. Specifically, these observations highlighted the need to understand how the deep equatorial ocean is energized. It was originally hypothesized that these currents could be explained as wind forced waves radiating downward from the surface (Wunsch 1977). While more recent data suggest that these flows may be steady (Eriksen 1985; Firing 1986), this does not diminish the need to understand the deep ocean's response to time varying surface wind forcing. For example, the annual cycle has been detected from time series measurements near the ocean bottom in the western equatorial Pacific (Eriksen 1981), annual Rossby wave variability has been observed in the upper 1000 m of the central equatorial Pacific (Lukas and Firing 1985), and there is a low vertical wavenumber spectrum associated with low frequency temporal variations in the eastern equatorial Pacific (Behringer 1984). It is not known to what extent this variability may be related to surface wind forcing, but studies that attempt to relate deep ocean energy to surface wind forcing by wave radiation should account for the various inhomogeneities of the media, especially the presence of mean currents.

The purpose of this paper is twofold: 1) to examine the effects of mean currents of the equatorial waveguide on the vertical propagation of wind forced low frequency Kelvin waves and 2) to determine the extent to which these waves can accelerate flows in the shallow

Corresponding author address: Dr. L. M. Rothstein, School of Oceanography, WB-10, University of Washington, Seattle, WA 98195.

Equatorial Undercurrent system. This paper is a natural extension of a few recent theoretical studies. McCreary (1984) forced a linear, continuously stratified equatorial ocean model with a zonal patch of wind oscillating at the annual period. For the case of a linear background stratification and in the absence of mean currents, the Kelvin wave response took the form of well-defined beams of equatorial wave energy that propagated both eastward and downward into the deep ocean. The geometry of the beam is related to the geometry and frequency of the forcing as well as the background stability frequency (Rothstein et al. 1985).

The effects of a sharp, near surface pycnocline on the transmission of periodically forced equatorial Kelvin waves was studied by Rothstein et al. (1985). They found that, for realistic choices of pycnocline structures, most of the wind forced energy propagates directly through the pycnocline and enters the deep ocean. These results were strongly dependent on the assumed amplitude of deep vertical mixing, consistent with the results of Gent and Luyten (1985). These analytic studies, however, neglected the interaction of the equatorial waves with the strongly sheared currents of the equatorial region.

There have been studies addressing the equatorial oceanic wave–mean flow interaction problem (Philander 1979; McPhaden and Knox 1979) but, until recently, all of these have done so in the context of a one- or two-layered, reduced gravity model. This allows for satisfactory treatment of the effects of lateral mean shear on equatorial waves, but does not adequately account for the effects of the observed strong vertical shear, especially those associated with the South Equatorial Current–Equatorial Undercurrent system. In particular, these studies are limited in that they cannot directly investigate vertical energy propagation.

Recently, McPhaden et al. (1986, hereafter MPR) and McPhaden et al. (1987) investigated the interaction of baroclinic equatorial Kelvin waves with realistically sheared background zonal currents in a linearized, continuously stratified model. Both continuous vertical and horizontal mean shear were included. The model was forced with an imposed vertical velocity at the surface, designed to resonate with Kelvin wavelike solutions (see Wunsch 1977 for a similar treatment of the forcing). The bottom boundary was reflecting, allowing for the establishment of vertical modes. Their results indicate that the presence of a background zonal jet can significantly modify the structures and dispersion characteristics of baroclinic Kelvin waves depending on the speed and the spatial scales of the mean flow relative to those of the waves. MPR conclude that it may not be possible to set up energetic high vertical mode Kelvin waves in the equatorial ocean due to the presence of critical surfaces where the wave phase speed equals the mean flow speed. In this paper we extend MPR to explicitly examine the propagation of wind forced Kelvin waves through realistic mean currents.

In addition to modification of the waves by the mean currents, waves can also have an affect on the mean currents themselves, especially in the vicinity of critical surfaces. Wave momentum and heat transports tend to induce a mean zonal acceleration and a mean circulation in the meridional plane. These effects have been studied extensively by meteorologists and used to explain observations such as the quasi-biennial oscillation (Lindzen and Holton 1968; Holton and Lindzen 1972) and the sudden stratospheric warmings (Matsuno 1971; Holton 1976). A powerful diagnostic framework (albeit longitudinally averaged) for studying wave–mean flow interactions has been developed based on these effects (Boyd 1976; Andrews and McIntyre 1976; Edmon et al. 1980; McPhaden et al. 1986), and these formulations will be used here to help analyze the present problem.

This paper is organized as follows: Section 2 briefly revisits the model employed in our earlier work (MPR) and points out the important differences in the present formulation. This section also includes a different discussion of the dynamics of the wave-induced acceleration and meridional circulation than MPR. Section 3 briefly outlines the numerical techniques used to solve the system of equations, and section 4 presents the results for various mean current configurations. Section 5 concludes the paper with a summary and discussion.

2. Model formulation

a. Equations and boundary conditions

In this study we use the equatorial channel model described in MPR. Consider time-dependent fluctuations of frequency σ and zonal wavenumber k linearized about a zonally invariant geostrophic zonal mean flow, $U(y, z)$, on an equatorial β-plane. Perturbations about this background are assumed to be of magnitude $O(\epsilon)$, where ϵ is a dimensionless amplitude parameter and $\epsilon \ll 1$. The model ocean is hydrostatic, incompressible, and Boussinesq. The governing equations for wave perturbations in standard notation are given by

$$-ik(c-U)u + vU_y + wU_z - \beta yv + ikp = -ru + F \quad \text{(a)}$$

$$\beta yu + p_y = 0 \quad \text{(b)}$$

$$p_z = -g\rho/\rho_0 \quad \text{(c)}$$

$$iku + v_y + w_z = 0 \quad \text{(d)}$$

$$-ik(c-U)\rho + v\bar{\rho}_y + w\bar{\rho}_z = -r\rho. \quad \text{(e)} \quad (1)$$

where we have assumed damping in the form of Rayleigh friction and Newtonian cooling of equal magnitudes. We have made the long-wave approximation (McCreary 1985) which limits solutions to low frequency nondispersive Kelvin and Rossby waves. Only

the long Kelvin waves, whose zonal phase speed is $c = \sigma/k$, are considered in this study.

When waves encounter critical surfaces, the system (1) becomes singular as $r \to 0$. Damping removes this singularity by introducing a complex component to the Doppler-shifted phase speed; $c^* = (c - U + ir/k)$. The wave field is almost completely absorbed at critical surfaces in our model (by assumption), accelerating the background flow there via Reynolds stress transfers of energy and momentum (Booker and Bretherton 1967). With damping the wave field is attenuated not only by absorption into the background flow, but also by dissipation due to turbulent processes in a region of finite thickness enclosing the critical surface.

The model formulation used in this paper differs from MPR in three important respects. First, the bottom boundary is radiating rather than reflecting, i.e, the solid bottom boundary in MPR is replaced by $p_z = imp$ where p is pressure and m is the local vertical wavenumber given by Nk/σ in the absence of mean flow (N is the Väisälä frequency). This condition eliminates bottom reflections (and standing vertical modes) so that we can isolate downward energy flux through the upper ocean mean flows. Second, we look for solutions symmetric about the equator as in MPR, but the poleward boundary is fixed at 4°N rather than allowed to vary depending on the Rossby radius of deformation for a particular wave. The reason for this will be discussed in section 3. Third and most importantly, in this study the ocean is forced by a zonal wind stress. Meridional wind stress is assumed to be zero since it is not effective in exciting low frequency Kelvin waves.

b. *Wind forcing*

The zonal wind enters the problem as a body force. Here we specify the form of the forcing as

$$F(x, y, z, t) = \tau_0 X(x) Y(y) Z(z) \exp(-i\sigma t). \quad (2)$$

For our experiments we set $\sigma = 2\pi/(6\text{ mo})$ or $2\pi/\text{yr}$ and take the amplitude of the annual and semiannual harmonic as $\tau_0 = 0.2$ dyn cm^{-2} and 0.1 dyn cm^{-2}, respectively (Kessler, personal communication). The zonal structure of the zonal wind is idealized as

$$X(x) = \begin{cases} \cos(\pi x/\Delta x), & |x| < \Delta x/2 \\ 0, & |x| > \Delta x/2. \end{cases} \quad (2a)$$

This represents a patch of zonal wind of longitudinal extent Δx which we approximate by a synthesis of zonal wavenumbers as

$$X(x) = \sum_{j=-J/2}^{J/2} A_j \exp(ik_j x) \quad (2b)$$

where $k_j = jK$ and $K = 2\pi/\mathcal{L}$ is the fundamental wavenumber. The forcing spectrum, A_j, is shown in Fig. 1. The shape of this spectrum is a function of Δx and $\mathcal{L}$ and reveals a broadband forcing in zonal wavenumber. Equation (2b) gives the desired patch of wind but it necessarily repeats the pattern of (2a) with wavelength $\mathcal{L}$, i.e., the wind pattern (2b) is aliased with wavelength $\mathcal{L}$. The representation (2b) is convenient, however, as now the model is fully spectral in both time and longitude and the forcing can be directly imposed on the system (1) for each (σ, k) pair. For all the results of this paper, we set the wind patch $\Delta x =$ 2000 km and $\mathcal{L} =$ 30 000 km, which establishes the lowest nonzero zonal wavenumber of the response. While admittedly arbitrary, this low-wavenumber cutoff was chosen by considering the approximate width of the equatorial Pacific (15 000 km) in which one-half wavelength might reasonably be expected to fit. Higher wavenumber cutoffs would apply to the Atlantic and Indian oceans according to this rationale. Finally, we consider only the positive k_j harmonics of the response since we are interested only in the Kelvin waves in this paper. It was found that 20 zonal harmonics were sufficient to recover 94% of the variance of the desired 2000-km wide zonal patch of wind forcing. The individual phase speeds of those twenty zonal harmonics are recorded in Table 1 for both the annual and semiannual forcings and will be useful in interpreting the results.

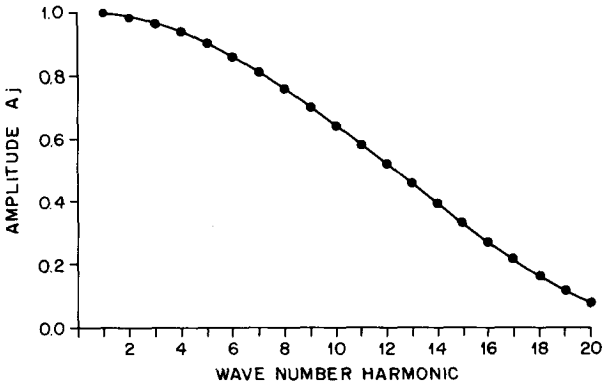

FIG. 1. Forcing spectrum, A_j, used to force the model ocean representing a zonal patch of zonal wind. The fundamental harmonic has a wavelength of 30 000 km.

The meridional structure of the zonal wind is taken as

$$Y(y) = \left[1 + \left(\frac{y}{\Delta y}\right)^2\right] \exp\left[-\left(\frac{y^2}{\Delta y^2}\right)\right] \quad (2c)$$

which gives a symmetrical wind about the equator. For all experiments in this paper, $\Delta y =$ 2000 km so that the wind has negligible curl ($Y(y) \sim 1$) in the model domain.

Finally, we take the depth structure of the zonal wind to be

$$Z(z) = \left(\frac{\pi}{2\Delta z}\right) \cos\left(\frac{\pi z}{2\Delta z}\right) \theta(z + \Delta z) \quad (2d)$$

where θ is the Heaviside step function. Equation (2d) represents a body force in the upper ocean over depth Δz below the surface. This tapered body forcing is chosen to avoid discontinuous vertical derivatives at the base of the mixed layer, Δz. Solutions did not change significantly for experiments using an untapered body force, suggesting that results are insensitive to the vertical structure of the forcing in the mixed layer (Gent 1987 reaches the same conclusion). For all experiments herein, $\Delta z = 50$ m, a value typical of the central equatorial Pacific.

c. *Induced mean currents and acceleration*

The noninteraction theorem (e.g., Boyd 1976; Andrews and McIntyre 1976; Holton 1983) provides a framework for evaluating the effects of wave driving of background flows. This theorem states that in the absence of friction, forcing, and critical layers, waves with stationary amplitudes should conserve wave action flux. An immediate consequence of this is that there will be no net exchange of momentum between the background flow and the wave field. If the conditions for noninteraction are violated, as they are for several of the cases to be examined in this paper, then equatorial waves are capable of accelerating background zonal currents on time scales much longer than the wave period. This can be expressed mathematically by examining the zonally averaged equation at $O(\epsilon^2)$:

$$U_t + (U_{0y} - \beta y)\chi_z - U_{0z}\chi_y = -\nabla \cdot \mathrm{EP} \quad \text{(a)}$$

$$\beta y U + P_y = 0 \quad \text{(b)}$$

$$P_{zt} - \beta y U_{0z}\chi_z - N_0^2\chi_y = r\left(\frac{\overline{p_z p_z}}{N_0^2}\right)_z \quad \text{(c)} \quad (3)$$

where

$$\nabla \cdot \mathrm{EP} = \left(\overline{uv} - U_{0z}\frac{\overline{vp_z}}{N_0^2}\right)_y + \left(\overline{uw} - (\beta y - U_{0y})\frac{\overline{vp_z}}{N_0^2}\right)_z \quad (4)$$

has come to be known as the Eliassen-Palm (EP) flux divergence (Andrews and McIntyre 1976) and χ is an $O(\epsilon^2)$ meridional streamfunction representing mean flow that is not compensated for by eddy momentum fluxes. The zero-order mean fields in (3) and (4) are distinguished by a zero subscript, the $O(\epsilon)$ fields are in lower case, and the $O(\epsilon^2)$ fields in upper case. An overbar denotes a zonal average over the fundamental wavelength $\mathcal{L}$. Equations (3) are the "transformed Eulerian mean" (TEM) equations of Boyd (1976) and Andrews and McIntyre (1976). This dynamical construct is attractive in that it represents the net wave forcing in a form that can be more easily interpreted in terms of an acceleration, U_t, i.e., the wave transports appear only in the zonal momentum equation. When wave momentum fluxes are not totally compensated by wave meridional heat fluxes, the EP-flux convergence can drive a mean acceleration, U_t, and/or a residual meridional circulation, χ.

TABLE 1. Phase speed of the individual zonal harmonics of the zonal wind forcing.

Zonal harmonic	Phase speed c (cm s^{-1})	
	Annual	Semiannual
1	97	193
2	48	96
3	32	64
4	24	48
5	20	39
6	16	32
7	14	28
8	12	24
9	11	21
10	10	19
11	9	18
12	8	16
13	7.5	15
14	7	14
15	6.5	13
16	6	12
17	5.5	11
18	5.3	10.7
19	5.1	10.2
20	4.8	9.6

We solve for the residual circulation, χ, by combining (3) into a single partial differential equation of the form

$$\mathcal{A}\chi_{yy} + \mathcal{B}\chi_{yz} + \mathcal{C}\chi_{zz} + \mathcal{D}\chi_z = \mathcal{E} \quad (5)$$

where

$$\mathcal{A} = 1$$

$$\mathcal{B} = 2\beta y U_{0z}/N_0^2$$

$$\mathcal{C} = -\beta y(U_{0y} - \beta y)/N_0^2$$

$$\mathcal{D} = \beta U_{0z}/N_0^2$$

$$\mathcal{E} = \frac{1}{N_0^2}\left\{\beta y(\nabla \cdot \mathrm{EP})_z - \left[r\left(\frac{\overline{p_z p_z}}{N_0^2}\right)_z\right]_y\right\}.$$

Equation (5) is elliptic [the discriminant of (5) is just the same as the $O(\epsilon)$ pressure equation (see Proehl et al. 1986)] and so χ, its normal derivative or some linear combination of the two, must be specified along the boundaries. Without a priori knowledge of χ, we take $\chi = 0$ along the boundaries. (See Andrews et al. 1987, section 3B for a discussion of the possible boundary conditions on χ.) This is the most sensible choice here, as we want to isolate wave driven mean field tendencies and hence want to avoid any direct forcing at $O(\epsilon^2)$.

The major advantage of the equations in this form is that the net wave forcing of the mean flow is now seen to be $-\nabla \cdot$ EP suggesting that contours of the EP-flux convergence (and EP vectors) will prove useful for diagnosing wave driving of mean zonal currents. In diagnosing these dynamics for the present problem, we will present the EP-flux vectors, the U_t field, and the induced residual meridional cell χ for the case of a background current consisting of the South Equatorial Current–Equatorial Undercurrent (SEC–EUC) system.

d. *Perturbation energy balance*

Although wave energy will not be conserved for waves in an inhomogenous moving medium (wave action flux is the appropriate conservative field according to Andrews and McIntyre 1976), the wave energy balance provides useful information on the various sources and sinks of wave energy. It also provides a check on the numerical accuracy of our results. For waves governed by (1), the zonally-averaged balance is

$$\underset{\text{(DIV)}}{(\overline{vp})_y + (\overline{wp})_z} = \underset{\text{(HS)}}{-(\overline{uv}U_y)} \underset{\text{(VS)}}{- (\overline{uw}U_z)} + \underset{\text{(DW)}}{\frac{\beta y}{N^2} U_z(\overline{vp}_z)} \underset{\text{(DS)}}{- 2r\overline{E^2}} \underset{\text{(W)}}{+ \overline{uF}} \quad (6)$$

where

$$\overline{E^2} = \frac{1}{2}[\overline{u^2} + \overline{v^2} + (\overline{p_z^2}/N^2)]$$

is the wave energy per unit zonal wavelength and we have dropped the zero subscript on U and N^2. Equation (6) represents an energetically stationary and zonally homogenous wave field by virtue of the specified harmonic x–t dependence in (1).

Integrating (6) over a closed contour including the surface leads to a bulk measure of wave energetics per unit mass. Because we have a radiating bottom boundary, there will be a net flux of energy through the bottom. The shorthand notation below each term in (6) indicating energy flux divergence (DIV), work on the O(1) horizontal (HS) and vertical (VS) shear, work on the O(1) meridional density gradient (DW), dissipation (DS), and work done by the wind (W) will be useful in later discussions.

3. Method of solution

Equations (1) are solved for each zonal wavenumber, k_j, by reducing the system to a single equation for the pressure. We write p-derivatives in finite difference form on an NY × NZ grid where NY is the number of grid points in the meridional half-plane ($\delta \leq y \leq L_B$) and NZ is the number of points over the depth range ($-H \leq z \leq 0$). In all cases, the upper 500 m is isolated for study by placing our radiation condition at 500 m. The first grid point in latitude is at $y = \delta < L = (c/\beta)^{1/2}$ instead of $y = 0$ to simplify the specifications of the gradient condition $\partial p/\partial y = 0$ at the equator. Here, c is the phase speed of the highest zonal harmonic. We require that p vanish at the poleward boundary $y = L_B = 400$ km and choose a resolution of 5 meters in the vertical and 20 km latitudinally. The poleward boundary remains fixed at L_B instead of allowing it to vary with zonal wavenumber as in MPR. We have chosen $L_B = 400$ km based upon comparisons with the analytical results of Rothstein et al. (1985) and the largest deformation radius expected from all our experiments. (The largest deformation radius is 310 km for the gravest semiannual harmonic.)

The problem reduces to solving NY × NZ simultaneous linear equations for the complex pressure field. A complete description of the numerical techniques used in solving this elliptic system can be found in Proehl et al. (1986).

Once we have solutions for each zonal wavenumber, $P_j(y, z)$, the complete x-dependence of the solutions is recovered by summing over k_j. Solutions were well converged for the 20 zonal harmonics used in our model. The final solution is therefore

$$p(x, y, z, t) = \sum_{j=1}^{20} P_j(y, z) \exp(ik_j x) \exp(-i\sigma t). \quad (7)$$

Note that the sum in (7) includes only nonzero zonal wavenumbers. The zero wavenumber component is vertically and horizontally unbounded and has a singularity in vertical energy flux (Gent 1987). Such a mode cannot be excited in the real ocean and hence this mode has been omitted from our solutions.

Comparisons between numerical solutions and known analytical solutions were excellent [see section 4.a(1)]. In the cases where no analytical solutions exist, a check on the solution was performed by increasing the resolution in both latitude and depth until convergence was obtained. A further test on the accuracy of the numerical solution over a range of r and U involved calculating u, v and w from (1) and substituting into the continuity equation. (Continuity was not used in deriving the velocity components so that this constitutes a consistency check on the solutions.) Generally, residuals were at most only a few percent in the mass budget. Similar accuracy was obtained in using the energy budget, (6), for consistency checks.

4. Results

This section shows solutions for various choices of background currents. The background zonal flow takes the analytical form of two Gaussian jets given by

$$U = U_1 \exp\left[\frac{-y^2}{2L_1^2}\right] \exp\left[\frac{-(z - z_{01})^2}{2H_1^2}\right] + U_2 \exp\left[\frac{-y^2}{2L_2^2}\right] \exp\left[\frac{-(z - z_{02})^2}{2H_2^2}\right]. \quad (8)$$

The speed and direction of the jets are contained in the amplitude factors U_1 and U_2 whereas meridional and depth scales are specified by L_1, L_2 and H_1, H_2, respectively. The jets are centered at depths z_{01} and z_{02}. The two jets in (8) allow for a somewhat crude representation of a background state containing both a surface South Equatorial Current and the Equatorial Undercurrent. For most of the calculations discussed here we have set $N^2(L_b, z)$ analytically to resemble an equatorial pycnocline (Fig. 2). [The exception is the benchmark experiment which is cast in a constant $N^2(L_b, z)$ ocean.] Table 2 lists the four cases of mean current configurations we will present in this paper.

For our purpose here, we specify mean currents that are stable with respect to the perturbations we are studying. This is accomplished by first making the long-wave approximation which filters the fastest growing equatorial instabilities from our solution (Philander 1976, 1978). Furthermore, we restrict our zero-order flows to satisfy

$$\left(\frac{N^2}{g}\beta y S\right)_y \neq 0; \qquad S = \left(1 - \frac{U_z^2}{N^2} - \frac{U_y}{\beta_y}\right) \quad (9)$$

on the meridional plane, i.e., the mean potential vorticity sensed by the wave field does not change sign. This is similar to the Rayleigh stability criterion for midlatitude barotropic flow except for the Richardson number dependence ($\mathrm{Ri} = N^2/U_z^2$) in S, which is a result of the ageostrophic divergent equatorial motions. Equation (9) is only approximate on the equatorial β-plane, however, since general stability criteria have yet to be developed for a continuously stratified equatorial ocean. (See Ripa and Marinone 1983 for these conditions in a reduced gravity, equatorial basin and also Long 1987 for a more general stability analysis.)

For all solutions, we plot contours of the *time-averaged* vertical energy flux in the equatorial plane, $\lambda(x, z)$, which is equivalent to $\frac{1}{2}\,\mathrm{Re}(wp^*)/g$, where p^* is the complex conjugate of p, and $\mathrm{Re}(wp^*)$ is the real part of wp^*. This quantity will clearly show the location of the wind forced beams of time-periodic Kelvin wave energy and the modification to this structure due to mean currents and friction. It is also useful to define a measure of the contributions of the individual longitudinal harmonics, k_j, to the total solution. We will thus calculate

$$\Lambda_j(z) = \Lambda(k_j) = \frac{1}{\mathrm{NY}} \int_{L_B}^{0} \frac{|W_j P_j^*|}{g}\, dy \quad (10)$$

which is equivalent to a time, zonal and latitudinally averaged wavenumber spectrum at depth z. The energy

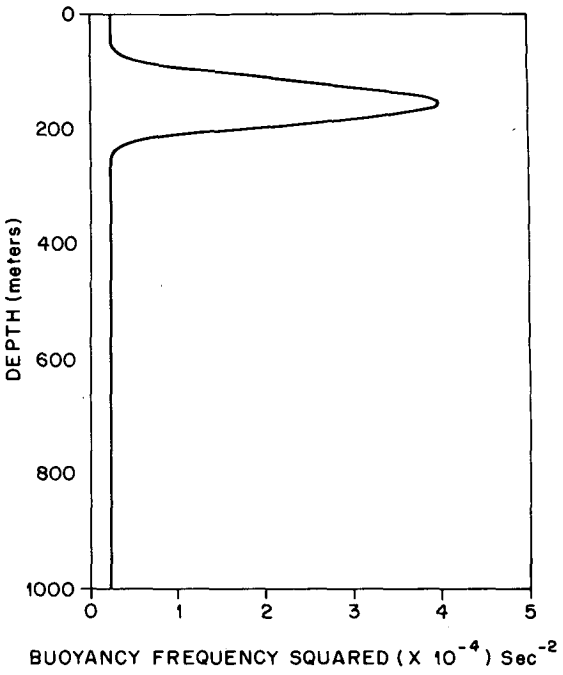

FIG. 2. Stability frequency squared as a function of depth at $y = L_b$ for most experiments.

TABLE 2. Range of background current configurations examined.

Case	$2\pi/\sigma$	U_1 (cm s^{-1})	L_1 (km)	H_1 (m)	z_{01} (m)	U_2 (cm s^{-1})	L_2 (km)	H_2 (m)	z_{02} (m)	r^{-1} (yr)	Displayed in Fig.
1	a b	0	—	—	—	0	—	—	—	0	3
2	b	0	—	—	—	0	—	—	—	5	4
3	b	75	150	125	200	0	—	—	—	5	6
4	a b	70	150	125	200	−40	300	75	0	5	10

a: Annual
b: Semiannual

flux contours and the spectral amplitudes from each experiment have been normalized with the maximum values found from all experiments. This facilitates comparisons among the different cases. The maximum values occurred for Cases 1a and 1b (Figs. 3c and 3b) representing the inviscid, no-mean flow annual and semiannual cases.

a. Solutions for U = 0

We first present the results for a resting background state for both inviscid ($r = 0$) and viscous ($r = 1/5$ yr) fluids (Table 2, Cases 1 and 2). Results for both annual and semiannual wind forcing are presented for Case 1. These cases illustrate how Kelvin wave energy can propagate into the deep ocean through a pycnocline, and the effect that friction and forcing frequency have on that propagation. These are control cases against which we will compare the results for more realistic background states.

1) INVISCID OCEAN

Figures 3a–c show the vertical energy flux, λ, and the zonal wavenumber spectrum, Λ_j(500 m) for Case 1 in a section that extends 15 000 km zonally, approximately the longitudinal extent of the equatorial Pacific Ocean. The figures illustrate the effect of a realistic pycnocline on the downward propagation of the Kelvin beam (Figs. 3a and 3b) and the effect of the forcing frequency on the geometry of the beam (Figs. 3b and 3c).

The slope of the ray paths as predicted analytically is simply $\theta = \tan^{-1}(\sigma/N_b)$ and so the semiannual signal

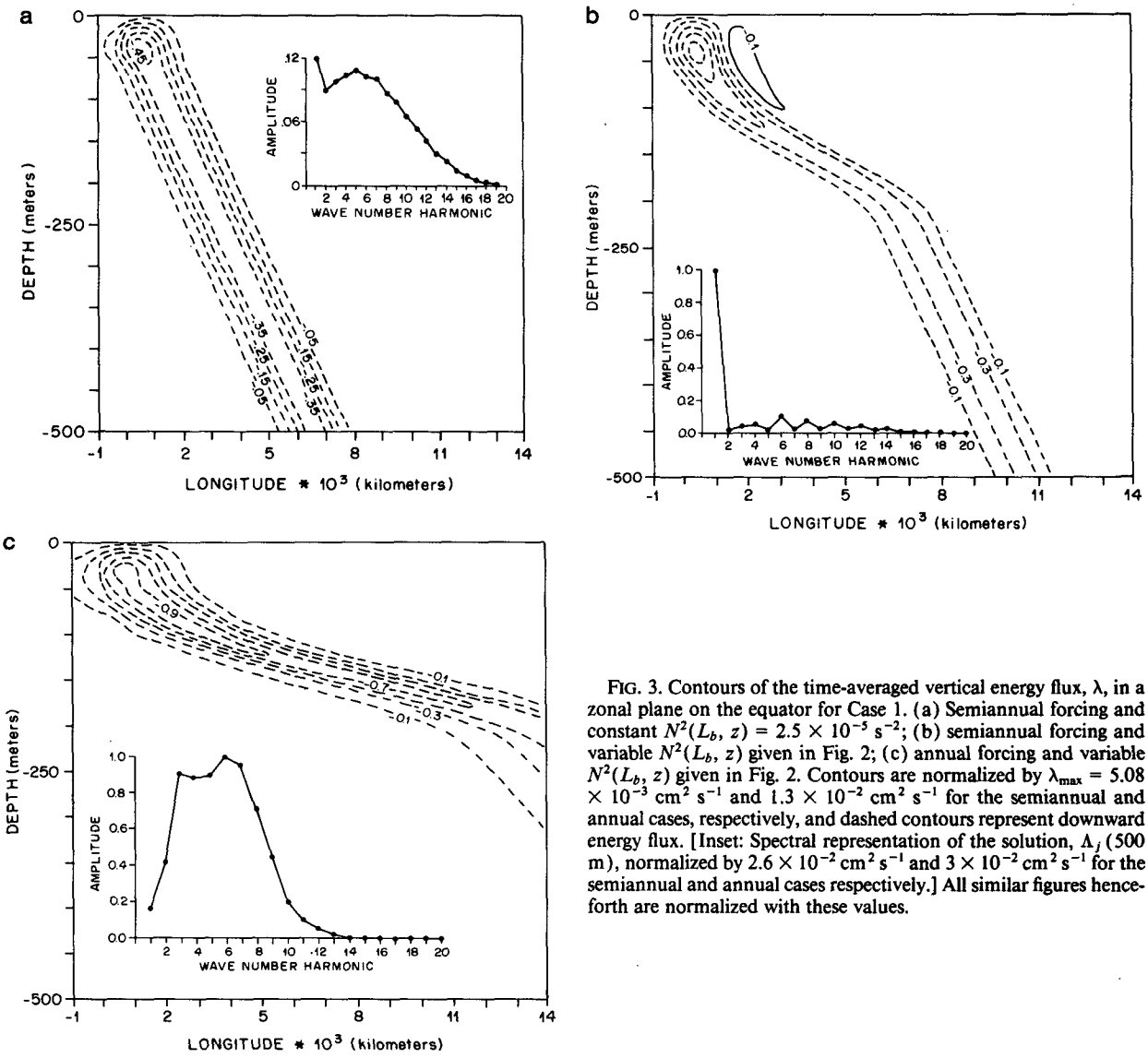

FIG. 3. Contours of the time-averaged vertical energy flux, λ, in a zonal plane on the equator for Case 1. (a) Semiannual forcing and constant $N^2(L_b, z) = 2.5 \times 10^{-5}$ s^{-2}; (b) semiannual forcing and variable $N^2(L_b, z)$ given in Fig. 2; (c) annual forcing and variable $N^2(L_b, z)$ given in Fig. 2. Contours are normalized by $\lambda_{max} = 5.08 \times 10^{-3}$ cm^2 s^{-1} and 1.3×10^{-2} cm^2 s^{-1} for the semiannual and annual cases, respectively, and dashed contours represent downward energy flux. [Inset: Spectral representation of the solution, Λ_j(500 m), normalized by 2.6×10^{-2} cm^2 s^{-1} and 3×10^{-2} cm^2 s^{-1} for the semiannual and annual cases respectively.] All similar figures henceforth are normalized with these values.

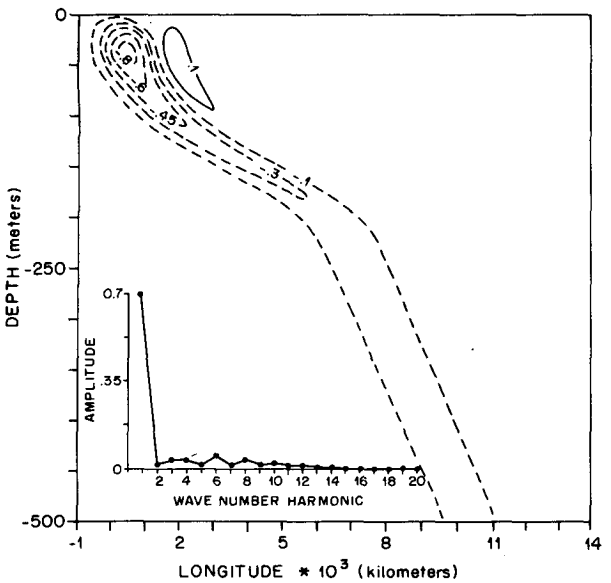

FIG. 4. As in Fig. 3b except for the frictional amplitude of Case 2.

should be found deeper than the annual signal at a given longitude. Similarly, the beam should be found shallower at a given longitude for the case of a beam propagating through a pycnocline. The numerical results of Fig. 3 clearly show this and also retrieve the analytical results of Rothstein et al. (1985), who showed that realistic pycnoclines do not prohibit wind forced energy from penetrating into the deep equatorial ocean.

The response spectra for all three cases are also presented in Fig. 3 (inset). For the constant N^2 results of Fig. 3a, the only vertical scale imposed on the problem is that of the depth of the body forcing. The broad spectral peak of Fig. 3a is a manifestation of this 50 m scale, where the vertical wavenumber $m = Nk/\sigma$ for these linear waves and many zonal wavenumbers have vertical scales near 50 m for this frequency. (The range of vertical scales for zonal wavenumbers 4 through 10 is 96 to 38 m.) The effect on this spectral structure of adding a pycnocline is shown in Fig. 3b. Based on the maximum N^2 ($=4 \times 10^{-4}$ s^{-2}), the gravest zonal wavenumber has a vertical scale of $\sim$100 m at the semiannual period. This vertical scale corresponds closely to the depth of maximum N^2 variability (Fig. 2) and thus there is a sharp spectral peak at the gravest wavenumber. Finally, decreasing the frequency shifts the spectral peak to higher wavenumber (Fig. 3c). For this case, the gravest zonal wavenumber has a vertical scale of 48 m based on the maximum N^2, a scale which is not a very good match with the scale of N^2 variability. (Lower wavenumbers would presumably peak to reflect this scale.) It is likely that the broad spectral peak of Fig. 3c is a manifestation of a combination of scales set by an average N^2 and perhaps the body force depth.

Due to the absence of dissipation and direct forcing in the deep ocean in this example, the waves do not drive a mean current below the mixed layer. Direct forcing in the surface layer does, however, locally induce a mean meridional circulation and will also tend to accelerate a zonal mean flow in the mixed layer. This breakdown of non-acceleration in the directly forced region has been known for some time (Andrews and McIntyre 1976; Boyd 1976) but has received little detailed analysis (see Colin de Verdiere 1980, for a midlatitude discussion). Since we wish to focus on wave–mean current interactions in this paper, the details of the directly forced region with respect to mean field tendencies will not be discussed in detail.

2) EFFECTS OF FRICTION

The effect of friction on the vertical energy flux of the Kelvin beam (Case 2) has been discussed at length in Rothstein et al. (1985). Here we present numerical results to illustrate the effect that a Rayleigh damping time of 5 years has on the structure of the beam (Fig. 4) for the semiannual case of Fig. 3b. As expected, the beam decays as it propagates into the deep ocean. Friction is weak enough that the beam structure is not

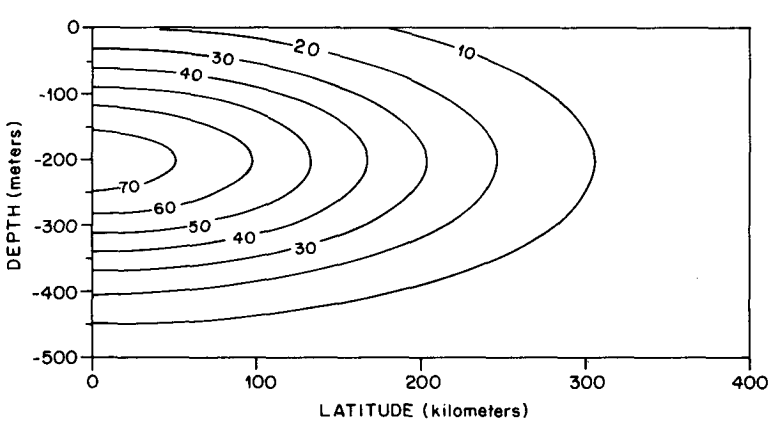

FIG. 5. Background zonal flow (U, in cm s^{-1}) for Case 3.

completely destroyed in the deep ocean. Notice also that the spectral shape, evaluated at the bottom, is quite similar to Fig. 3b, but the maximum response amplitude is reduced by 70% and the higher zonal harmonics are somewhat reduced relative to the lower harmonics. From now on, all solutions will be for a frictional damping of 5 years. This amplitude of dissipation, in the absence of mean currents, does not prohibit the beam from reaching the bottom boundary.

b. Solutions with mean background currents

1) AN EASTWARD UNDERCURRENT

We now wish to study the corresponding dynamics when the background state is no longer at rest. For Case 3, we investigate the effects of an eastward equatorial current with a maximum speed of 75 cm s^{-1} (Fig. 5) to illustrate the adjustment of the Kelvin beam to mean current shear. The location of the core of the eastward current is taken to be at 200 m. The decay scales are chosen so that the eastward current extends to the surface, essentially vanishes below 500 m and is confined to approximately 3° of the equator. This is clearly an attempt to isolate the effects of an Equatorial Undercurrent.

Figure 6 shows downward energy flux of the semiannual Kelvin beam into the mean current (contours of the mean current are superimposed). The beam enters the mean flow immediately in the forced region where it encounters multiple critical layers (one for each harmonic higher than the second) and is rapidly attenuated below. The phase speed of the third zonal harmonic comprising the beam is 64 cm s^{-1} (Table 1) so that only harmonics lower than this have no critical

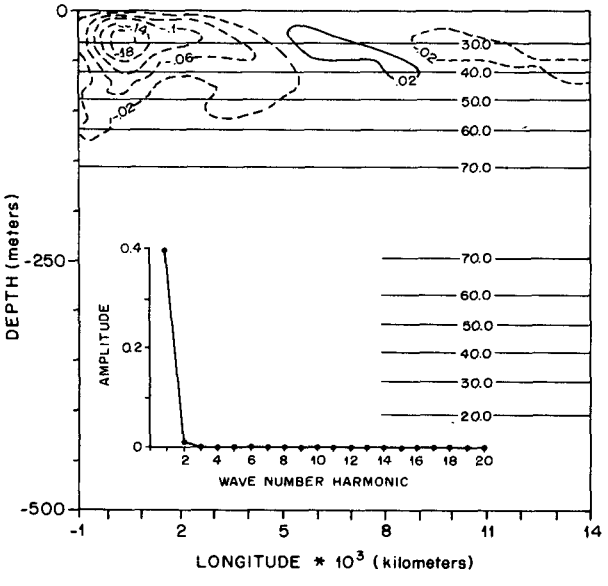

FIG. 6. As in Fig. 4 except for the mean background current of Case 3. Mean current contours, in cm s^{-1}, are superimposed.

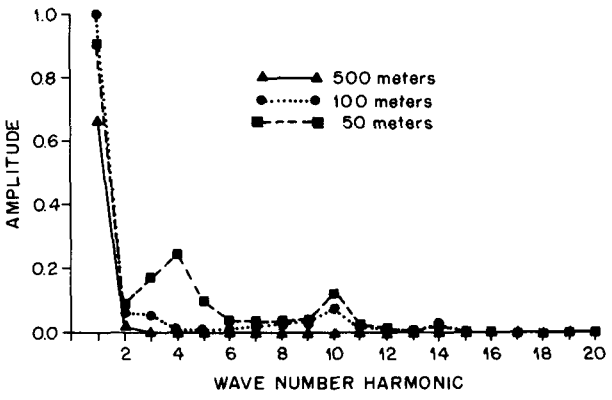

FIG. 7. Spectral representation of the solution of Case 3 at various depths, normalized to $\Lambda_{max} = 1.66 \times 10^{-2}$ cm^2 s^{-1}.

layer in the domain. As the beam encounters the current, most of the zonal harmonics comprising the structure of the beam will therefore be strongly damped and/or absorbed. Only a fraction of the original beam energy can penetrate the current. These effects are clearly illustrated by the wavenumber spectra, Λ_j (500 m) (Fig. 6, inset), where some amplitude remains only in the first and second harmonics.

There is some indication of reflections in the upper ocean for this case (see Fig. 6 again) where attention is drawn to an upward flux of energy immediately to the east of the main beam of energy and another downward energy flux region still farther east. To analyze this we compare the spectra at various depths (Fig. 7). As the Kelvin beam encounters the model undercurrent, the response loses energy in the higher harmonics. In this case, however, there is a secondary peak at 50 m in zonal harmonic 4 and a weaker peak at harmonic 10, implying preferred response scales above the undercurrent core. (The forcing spectrum, Fig. 1, shows no preference for this scale.) The vertical scale associated with the fourth harmonic, based on the linear Kelvin wave dispersion relation ($m = Nk/\sigma$) is 96 m where we have taken N^2 (L_b, 50 meters) $= 2.5 \times 10^{-5}$ s^{-2}. From Fig. 6 we notice that the depth of maximum shear occurs at approximately 100 m suggesting that this shear might act as a reflecting surface for the fourth harmonic. It is not obvious how to interpret the secondary peak at harmonic 10, but presumably this is associated with a combination of a preferred mean shear scale and a mean N^2 scale.

The main result of this case is that the semiannual Kelvin beam is substantially modified by a mean eastward current. Not only is surface forced energy directly impeded from reaching the deep ocean but very little energy propagates eastward away from the wind patch. The response is relatively localized.

The energy budget for this case is presented in Fig. 8a. The wind input is balanced by bottom radiation, frictional dissipation, and exchanges with the mean

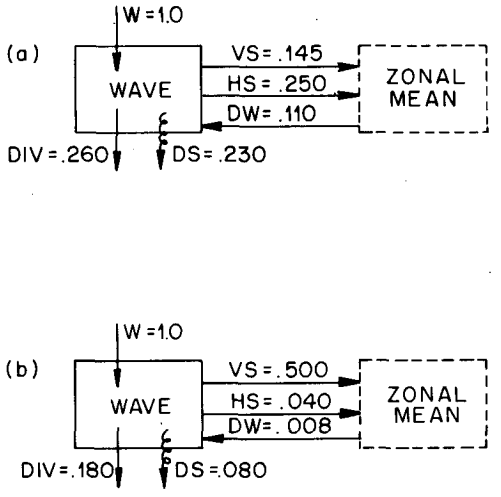

FIG. 8. Integrated wave energy balance for (a) Case 3 and (b) Case 4b. Integration is over the entire meridional plane and zonally averaged. Values are normalized to the wind energy input. See text for discussion of various terms.

current in roughly equal proportions. The waves are drawing energy by working on the mean meridional density gradient and losing energy via working on the vertical and horizontal mean shears, consistent with MPR. The largest energy loss to the mean current is through work done on horizontal shear with the waves losing 25% of their energy in this manner.

2) SEC–EUC CASE

We conclude our experiments with a case intended to resemble the South Equatorial Current–Equatorial Undercurrent system (Fig. 9). For Case 4 we therefore include a westward surface flow above the eastward current of Case 3. This configuration of mean currents increases the vertical shear in the upper ocean compared to Case 3, and this will be seen to have a major impact on the energetics.

The vertical energy flux through the mean currents is presented in Fig. 10 along with the wavenumber response spectrum, Λ_j (500 m) for both the semiannual (10a) and annual (10b) cases. The Kelvin beam refracts relatively cleanly through the surface westward flow and enters the eastward flow, where critical surfaces are again encountered for all but the first two zonal harmonics in the semiannual case and all but the gravest zonal harmonic for the annual case (see Table 1 and the spectra of Fig. 10). Once it reaches the eastward flow, the results are qualitatively similar to Case 3. The main effect of the westward flow is to refract the beam slightly west of the position it would occupy in the absence of surface westward flow. Again, the semiannual signal penetrates slightly deeper than the annual signal. The structures are qualitatively quite similar, however. The energy budget (Fig. 8b) now reveals that the work done against the mean vertical current shear dominates the energetics and continues to draw energy from the wave field. The implications of this result with respect to modeling equatorial wave–mean flow interactions will be discussed in the next section.

It is interesting to examine the mean field tendencies for the semiannual case. Figure 11a presents the EP-flux vectors superimposed on the mean current contours in the upper 250 m and Fig. 11b shows U_t. The EP-flux vectors show that the strong convergence occurs on the equator and well above the eastward current core. Notice the off-equatorial multicell pattern of U_t, which is due to the body forcing. However, the maximum U_t appears on the equator below the forced region and is due to the presence of critical surfaces in the undercurrent. There is a large local acceleration of the zonally averaged mean current of 196 cm s^{-1}/yr at about 75 m. The average U_t between 60 and 125 m is about 100 cm s^{-1}/yr, equivalent to a stress of 0.02 dyn cm^{-2}, or about 20% of the semiannual wind stress amplitude. The tendency of such a stress (and hence induced U_t) would be to move the eastward current core upward in the water column if this effect were unbalanced by other sinks of momentum.

The induced residual meridional circulation, Fig. 12, reveals the directly wind forced patterns with an additional and much smaller residual circulation induced above the core of the eastward jet. The amplitude of this circulation in the mixed layer is only about 0.4 cm s^{-1} for the meridional velocity, however, and is about an order smaller below the mixed layer.

5. Summary and discussion

A numerical model was designed to study the effects of the strong, near surface shears associated with the equatorial current system on energy transmission of time-periodic equatorial Kelvin waves into the deep ocean. The model is confined to the long wavelength, low frequency region of dispersion space. Damping takes the form of Rayleigh friction and Newtonian cooling and is necessary to allow for parameterizing critical surface effects. Annual and semiannual vertically propagating equatorial Kelvin waves forced by a longitudinal patch of zonal wind are isolated from the

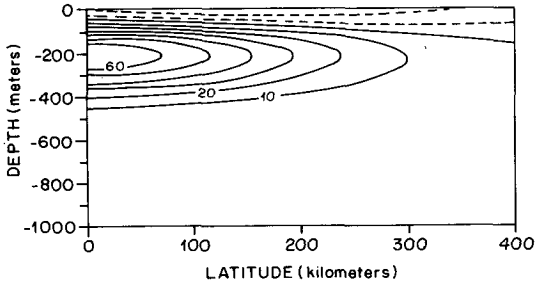

FIG. 9. Background zonal flow (U, in cm s^{-1}) of Case 4.

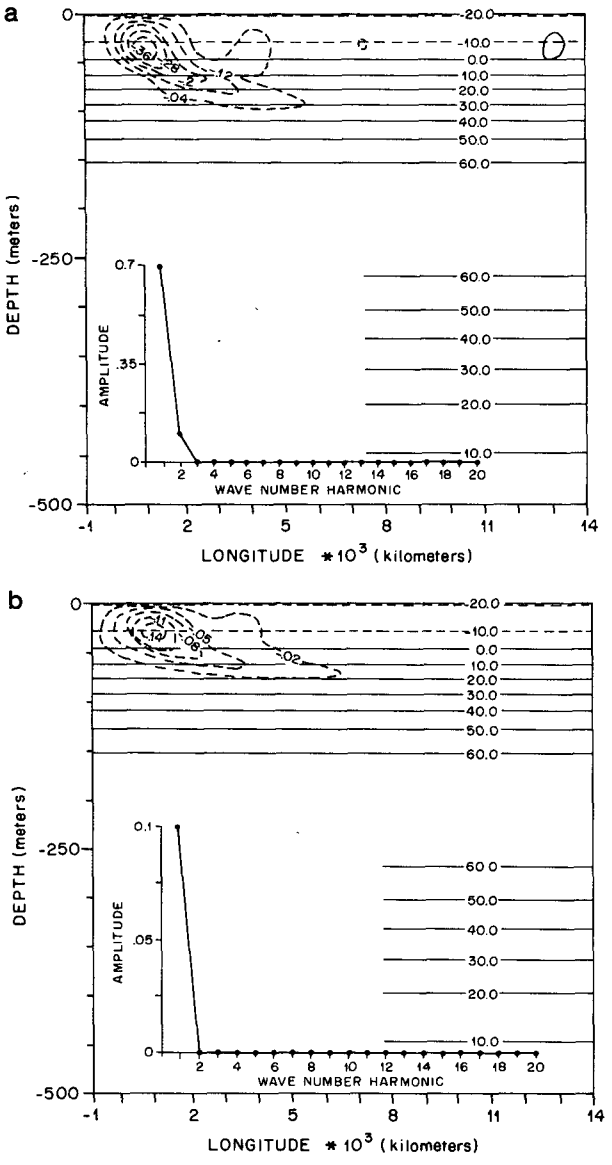

FIG. 10. As in Fig. 4 except for the mean background current of Case 4. Mean current contours, in cm s^{-1}, are superimposed. (a) Semiannual forcing. (b) Annual forcing.

complete response, and their energy transmission into the deep ocean is investigated as a function of mean shear amplitude and geometry and wind forcing frequency.

In the absence of strong mean flows, well defined beams of energy propagate eastward and vertically toward the deep ocean. However, the presence of critical surfaces inhibit this energy from reaching the deep ocean. These effects are illustrated by examining the downward energy flux, λ, and the wavenumber spectrum, $\Lambda_j(z)$, of the beam. The beam of energy can be thought of as composed of a number of zonal harmonics, each traveling at a different phase speed. When the current amplitude is large enough, components within the beam will encounter critical surfaces where a large exchange of energy and momentum can take place with the mean current via Reynolds stress transfers. The structure of the response spectrum will change for different configurations of mean currents, as shown in Fig. 13 which is a summary of Cases 2 (no mean current) and 4 (SEC–EUC case). Critical layer absorption and enhanced dissipation is illustrated as a diminution of wave energy at the higher zonal harmonics. As the mean current speed increases, these effects become more pronounced.

The system energetics afford another valuable tool for understanding these interactions. As the mean cur-

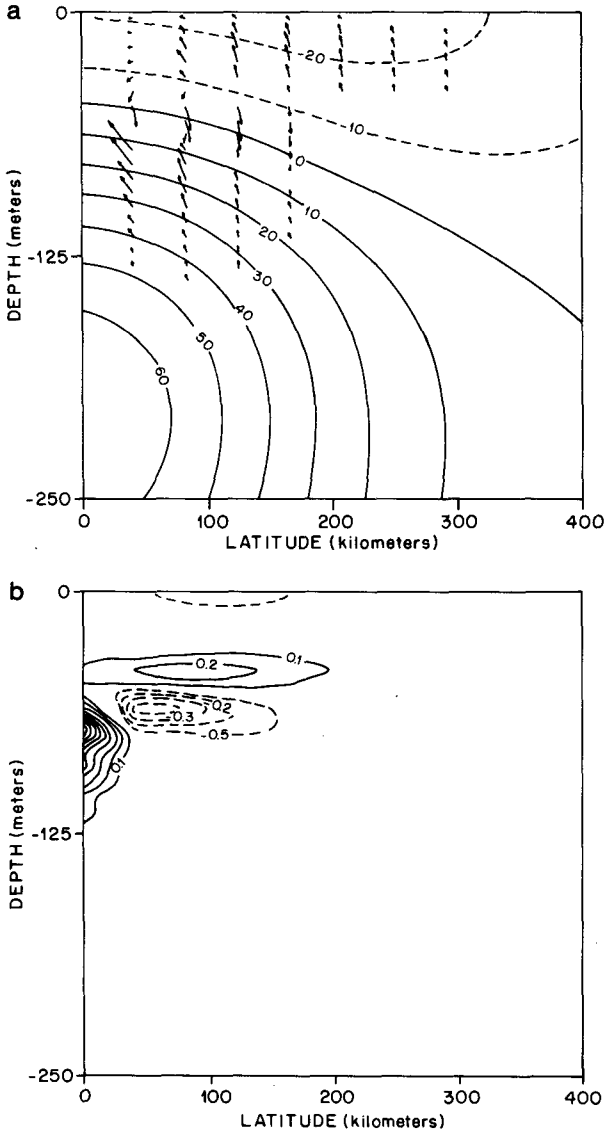

FIG. 11. (a) EP-flux vectors and (b) the induced $O(\epsilon^2)$ zonal acceleration in the uppermost 250 m for Case 4. Contours of acceleration have been normalized with $(U_t)_{max}$ = 196 cm s^{-1}/yr.

rent configuration is changed, energy exchanges with the various mean current shears change. In all cases, the Kelvin waves lose energy by working against both the mean vertical and horizontal shear, with the loss to vertical shear dominating the SEC–EUC case. This highlights a major limitation of the layer models for examining wave–mean flow interactions in the equatorial ocean. The vertical shear in these models is confined to infinitesimally thin interfaces which is an unrealistic representation of oceanic shears.

We find that the presence of critical surfaces above the undercurrent core results in significant mean field accelerations, equivalent, for example, to approximately 20% of the semiannual wind stress in our Case 4b. This would imply a slow upward movement of the core if the acceleration were not balanced by a sink of momentum. Presumably such a sink exists in the real ocean since the undercurrent is not observed to shoal continuously. However, our model is too simplistic to describe the full equilibrium balance of the Equatorial Undercurrent. The periodic body forcing used in this study also induces mean acceleration and residual meridional circulation in the directly forced region away from critical surfaces, as the non-interaction theory predicts.

The primary implication of these results with regard to observations in the equatorial waveguide is that low frequency Kelvin waves will find it difficult to propagate large zonal and vertical distances without encountering critical surfaces. Higher frequency Kelvin waves, i.e., those associated with westerly wind bursts in the western equatorial Pacific Ocean (Knox and Halpern 1982; Lukas et al. 1984; McPhaden et al. 1988), will be less affected by the mean currents. Of possible importance,

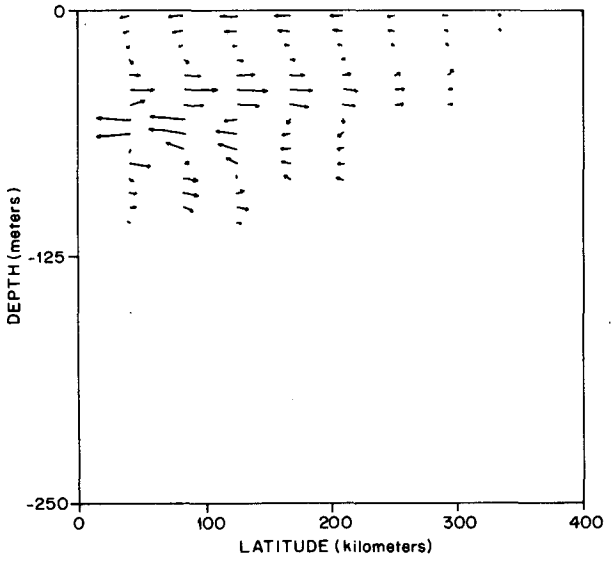

FIG. 12. The induced mean residual meridional circulation in the upper 250 m for Case 4b. The maximum meridional velocity is 0.4 cm s^{-1}.

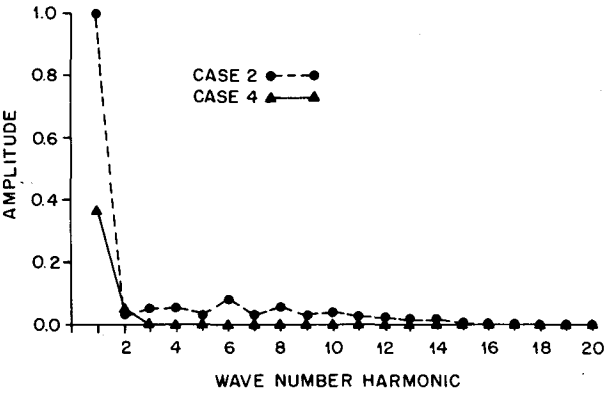

FIG. 13. Comparison of the spectral representation of the solution at $z = -500$ m for Cases 2 and 4b normalized to $\Lambda_{max} = 1.8 \times 10^{-2}$ cm^2 s^{-1}.

then, are times when the undercurrent disappears at certain longitudes (Firing et al. 1983; Halpern 1983), perhaps providing a window through which Kelvin wave energy might pass to the deep ocean. Such a situation might be more relevant to the Indian Ocean, in which a permanent Equatorial Undercurrent is not found.

Acknowledgments. We would like to thank an anonymous reviewer, whose comments improved the final paper. This work was supported by the National Science Foundation under Grant OCE-8700017.

REFERENCES

Andrews, M. E., and D. G. McIntyre, 1976: Planetary waves in horizontal and vertical shear: The generalized Eliassen-Palm relation and the mean zonal acceleration. *J. Atmos. Sci.*, **33**, 2031–2048.

——, J. R. Holton and C. B. Leovy, 1987: *Middle Atmosphere Dynamics*, Academic Press, 489 pp.

Behringer, D. W., 1984: Equatorial modes in the eastern Pacific (85°W). *J. Geophys. Res.*, **89**, 3729–3731.

Booker, J. R., and F. P. Bretherton, 1967: The critical layer for internal gravity waves in a shear flow. *J. Fluid Mech.*, **27**, 513–539.

Boyd, J. P., 1976: The noninteraction of waves with the zonally averaged flow on a spherical earth and the interrelationships of eddy fluxes of energy, heat and momentum. *J. Atmos. Sci.*, **33**, 2286–2291.

Bretherton, F. P., and C. J. R. Garrett, 1968: Wavetrains in inhomogeneous moving media. *Proc. Roy. Soc. London*, **A302**, 529–554.

Colin de Verdiere, A., 1980: Quasi-geostrophic turbulence in a rotating homogeneous fluid. *Geophys. Astrophys. Fluid Dyn.*, **15**, 213–251.

Edmon, H. J., B. J. Hoskins and M. E. McIntyre, 1980: Eliassen-Palm cross sections for the troposphere. *J. Atmos. Sci.*, **37**, 2600–2616.

Eriksen, C. C., 1981: Deep currents and their interpretation as equatorial waves in the western Pacific. *J. Phys. Oceanogr.*, **11**, 48–70.

Eriksen, C. C., 1985: Moored observations of deep low frequency motions in the central Pacific Ocean: Vertical structure and interpretations as equatorial waves. *J. Phys. Oceanogr.*, **15**, 1085–1113.

Firing, E., 1987: Deep zonal current in the central equatorial Pacific. *J. Mar. Res.*, **45**, 791–812.

——, R. Lukas, J. Sadler and K. Wyrtki, 1983: Equatorial undercurrent disappears during the 1982–1983 El Niño. *Science*, **222**, 1121–1123.

Gent, P. R., 1987: Forcing and friction effects on vertically propagating waves in the equatorial oceans. *J. Phys. Oceanogr.*, **17**, 1897–1908.

——, and J. R. Luyten, 1985: How much energy propagates vertically in the equatorial oceans? *J. Phys. Oceanogr.*, **15**, 997–1007.

Halpern, D., 1983: Upper ocean current and temperature observations along the equator west of the Galapagos Islands before and during the 1982–1983 ENSO event. *Proc. Workshop on El Niño–Southern Oscillation,* Miami, FL, U.S. Govt. Printing Office, Washington, DC, 59–92.

Hayes, S. P., and H. B. Milburn, 1980: On the vertical structure of velocity in the eastern tropical Pacific. *J. Phys. Oceanogr.*, **10**, 633–635.

Holton, J. R., 1976: A semi-spectral numerical model for wave–mean flow interactions in the stratosphere: Application to the sudden stratospheric warmings. *J. Atmos. Sci.*, **33**, 1639–1649.

——, 1983: The stratosphere and its links to the troposphere. *Large-Scale Dynamical Processes in the Atmosphere*, B. J. Hoskins and R. P. Pearce, Eds., Academic Press.

——, and R. S. Lindzen, 1972: An updated theory for the quasi-biennial cycle of the tropical troposphere. *J. Atmos. Sci.*, **29**, 1076–1080.

Knox, R. A., and D. Halpern, 1982: Long range Kelvin wave propagation of transport variations in Pacific Ocean equatorial currents. *J. Mar. Res.*, **40**(Suppl), 329–339.

Lindzen, R. S., and J. R. Holton, 1968: A theory of the quasi-biennial oscillation. *J. Atmos. Sci.*, **25**, 1095–1107.

Long, B., 1987: On the stability of steady ideal fluid flow. *Ocean Modelling*, **73**, 1–6.

Lukas, R., and E. Firing, 1985: The annual Rossby wave in the central equatorial Pacific Ocean. *J. Phys. Oceanogr.*, **15**, 55–67.

——, S. Hayes and K. Wyrtki, 1984: Equatorial sea level response during the 1982–83 El Niño. *J. Geophys. Res.*, **89**, 10 524–10 430.

Luyten, J. R., and J. C. Swallow, 1976: Equatorial undercurrents. *Deep-Sea Res.*, **23**, 909–1001.

McCreary, J. P., Jr., 1984: Equatorial beams. *J. Mar. Res.*, **42**, 395–430.

——, 1985: Modeling equatorial ocean circulation. *Annual Review of Fluid Mechanics*, Vol. 17, Annual Reviews, 359–409.

McPhaden, M. J., and R. A. Knox, 1979: Equatorial Kelvin and inertio-gravity waves in zonal shear flow. *J. Phys. Oceanogr.*, **9**, 263–277.

——, J. A. Proehl and L. M. Rothstein, 1986: The interaction of equatorial Kelvin waves with realistically sheared zonal currents. *J. Phys. Oceanogr.*, **16**, 1499–1515.

——, J. A. Proehl and L. M. Rothstein, 1987: On the structure of low-frequency equatorial waves. *J. Phys. Oceanogr.*, **17**, 1555–1559.

——, H. P. Freitag, S. P. Hayes, B. A. Taft, Z. Chen and K. Wyrtki, 1988: The response of the equatorial Pacific to a westerly wind burst in May 1986. *J. Geophys. Res.*, in press.

Matsuno, T., 1971: A dynamical model of the stratospheric sudden warming. *J. Atmos. Sci.*, **28**, 1479–1494.

Philander, S. G. H., 1976: Instabilities of zonal equatorial currents. *J. Geophys. Res.*, **81**, 3725–3735.

——, 1978: Instabilities of zonal currents, 2. *J. Geophys. Res.*, **83**, 3679–3682.

——, 1979: Equatorial waves in the presence of the Equatorial Undercurrent. *J. Phys. Oceanogr.*, **9**, 254–262.

Proehl, J. A., M. J. McPhaden and L. M. Rothstein, 1986: A numerical approach to equatorial oceanic wave–mean flow interactions. *Advanced Physical Oceanographic Numerical Modelling*, J. J. O'Brien, Ed., 111–126.

Ripa, P., and S. G. Marinone, 1983: The effect of zonal currents on equatorial waves. *Hydrodynamics of the Equatorial Ocean*, C. J. C. Nihoul, Ed., Elsevier Science, 219–317.

Rothstein, L. M., D. W. Moore and J. P. McCreary, 1985: Interior reflections of a periodically forced equatorial Kelvin wave. *J. Phys. Oceanogr.*, **15**, 985–996.

Wunsch, C., 1977: Response of an equatorial ocean to a periodic monsoon. *J. Phys. Oceanogr.*, *J. Phys. Oceanogr.*, **7**, 497–511.